Mechanism of Carbon Monoxide Oxidation by the Carbon Monoxide Dehydrogenase/Acetyl-CoA Synthase from *Clostridium thermoaceticum*: Kinetic Characterization of the Intermediates†

Javier Seravalli, Manoj Kumar, Wei-Ping Lu, and Stephen W. Ragsdale*

Department of Biochemistry, The Beadle Center, University of Nebraska, Lincoln, Nebraska 68588-0664

Received March 14, 1997; Revised Manuscript Received July 7, 1997⊗

ABSTRACT: Carbon monoxide dehydrogenase/acetyl-CoA synthase (CODH/ACS) from *Clostridium thermoaceticum* catalyzes (i) the synthesis of acetyl-CoA from a methylated corrinoid protein, CO, and coenzyme A and (ii) the oxidation of CO to CO_2. CO oxidation occurs at a Ni- and FeS-containing center known as cluster C. Electrons are transferred from cluster C to a separate metal center, cluster B, to external acceptors like ferredoxin. In the work described here, we performed reductive titrations of CODH/ACS with CO and sodium dithionite and monitored the reaction by electron paramagnetic resonance (EPR) spectroscopy. We also performed pre-steady-state kinetic studies by rapid freeze−quench EPR spectroscopy (FQ-EPR) and stopped-flow kinetics. Redox titrations of CODH/ACS revealed the existence of a UV−visible and EPR-silent electron acceptor denoted center S that does not appear to be associated with any of the other metal centers in the protein. Our results support the previous proposals [Anderson, M. E., & Lindahl, P. A. (1994) *Biochemistry 33*, 8702−8711; Anderson, M. E., & Lindahl, P. A. (1996) *Biochemistry 35*, 8371−8380] that the C_{red2} form of cluster C is two electrons more reduced than the C_{red1} form. The combined results from titrations and pre-steady-state studies were used to formulate a mechanism for CO oxidation, composed of the following steps: (i) CO binding to the [C_{red1},B_{ox},X_{ox}] state to yield a C_{red1}−CO complex; (ii) two-electron reduction of C_{red1} to C_{red2} concerted with CO_2 release; (iii) binding of a second CO molecule to the [C_{red2},B_{ox},X_{ox}] state to form a C_{red2}−CO complex; (iv) electron transfer from C_{red2}−CO to cluster B to form [C_{red2},B_{red},X_{red}] with concerted release of the second CO_2. Step iii competes with internal electron transfer from C_{red2} to B_{ox} and X_{ox}. At high CO concentrations, step iii is favored, whereas at low concentrations, only one CO molecule per turnover binds and undergoes oxidation. Closure of the catalytic cycle involves electron transfer from reduced enzyme to an electron acceptor protein, like ferredoxin. X_{ox} is a yet-uncharacterized electron acceptor that may be an intermediate in the reduction of center S. The C_{red2} state appears to be the predominant state of cluster C during steady-state turnover. The rate-determining step for the first half-reaction is step iv, while during steady-state turnover, it appears to be electron transfer to external electron acceptors.

Bacterial enzymes called carbon monoxide dehydrogenases can catalyze the interconversion of CO and CO_2 (Kumar & Ragsdale, 1996). This reaction allows bacteria to grow on CO as a sole carbon and energy source. There are two classes of CODHs, one that contains Ni and another that contains Mo. The Mo−CODHs are molybdopterin oxotransferases; the Ni-containing enzymes use a novel Ni−FeS cluster to catalyze CO oxidation. CO oxidation is mechanistically analogous to the metal-catalyzed water gas shift reaction, an important industrial process for H_2 generation. A key difference between the industrial and bacterial catalysis is that the enzyme is geared to produce electrons and protons (eq 1) instead of H_2, although it has been recently shown that, under certain conditions, CODH can also produce H_2 (Menon & Ragsdale, 1996; Santiago & Meyer, 1996; Bhatnagar *et al.*, 1987).

$$CO + H_2O \rightleftharpoons CO_2 + 2\,H^+ + 2\,e^- \qquad (1)$$

For certain classes of anaerobic organisms that use the Wood−Ljungdahl or acetyl-CoA pathway, both CO oxidation and CO_2 reduction are important. During bacterial growth on CO, CO must be oxidized to CO_2 to produce the methyl group of acetyl-CoA. When bacteria grow on other carbon sources, CO_2 must be reduced to CO to form the carbonyl moiety of acetyl-CoA (Menon & Ragsdale, 1996).

The carbon monoxide dehydrogenase/acetyl-CoA synthase (CODH/ACS)[1] from *Clostridium thermoaceticum* is an $\alpha_2\beta_2$ tetrameric bifunctional enzyme (Xia *et al.*, 1996) with a molecular mass of 310 kDa that catalyzes both CO oxidation and acetyl-CoA synthesis from a CODH-bound methyl group, CO, and CoA. Each $\alpha\beta$ heterodimer contains 2 Ni atoms, 11−13 Fe atoms, 1 Zn atom, and 14 sulfide ions (Ragsdale *et al.*, 1983) that are organized into three metal clusters, called clusters A, B, and C.

† Work described here was supported by NIH Grant GM 39451 to S.W.R.

* Address correspondence to this author: Phone (402)-472-8912; FAX (402)-472-7842; Email sragsdal@unlinfo.unl.edu.

⊗ Abstract published in *Advance ACS Abstracts,* September 1, 1997.

[1] Abbreviations: CODH, carbon monoxide dehydrogenase; CODH/ACS, carbon monoxide dehydrogenase/acetyl-CoA synthase; DTT, dithiothreitol; EPR, electron paramagnetic resonance; Fd, ferredoxin from *Clostridium thermoaceticum*; FMN, flavin mononucleotide; FQ-EPR, freeze−quench kinetics monitored by electron paramagnetic resonance spectroscopy; PCA/PCD, protocatechuic acid/protocatechuate dioxygenase.

S0006-2960(97)00590-4 CCC: $14.00 © 1997 American Chemical Society

CO oxidation requires clusters B and C, which that are housed in the β subunit of CODH/ACS. Cluster C appears to be the active site of CO oxidation and CO_2 reduction (Kumar *et al.*, 1993; Anderson *et al.*, 1993; Anderson & Lindahl, 1994; Qiu *et al.*, 1995). Several states of cluster C have been described. One of the aims of this paper is to assign the role of the different states of this unusual metal cluster. It is diamagnetic when oxidized (C_{ox}) and is paramagnetic with a net electron spin (S) of $^1/_2$ when reduced at relatively mild potentials to form the C_{red1} state ($E^{\circ\prime} = -220$ mV vs NHE). The EPR spectrum of C_{red1} has g values at 2.01, 1.81, and 1.65 ($g_{av} = 1.82$) and a maximum spin intensity of 0.30−0.40 spin per $\alpha\beta$ CODH/ACS dimer. A third stable $S = {}^1/_2$ state of this cluster, called C_{red2}, exhibits g values at 1.97, 1.87, and 1.75 ($g_{av} = 1.86$) and it is formed upon lowering the solution redox potential ($E^{\circ\prime} = -520$ mV) or by incubating with CO. C_{red2} is either isoelectronic or two electrons more reduced than C_{red1} (Anderson & Lindahl, 1994, 1996). Mössbauer spectroscopic studies (Hu *et al.*, 1996) showed that the oxidized form of cluster C contains a $[Fe_4S_4]^{2+}$ cluster with $S = 0$, while the C_{red1} form of the cluster contains an $S = {}^1/_2$ $[Fe_4S_4]^{1+}$ cluster. Upon incubation with anions, this cluster exhibits distinct EPR signals. Cyanide treatment elicits a signal with a g_{av} of 1.72 (Anderson *et al.*, 1993). When the enzyme is incubated with thiocyanate, signals with g_{av} values at 2.15 and 2.17 are observed (Seravalli *et al.*, 1995), while with azide, signals with a g_{av} value of 2.14 appear. All of these anion-dependent signals can replace the $g_{av} = 1.82$ signal from the C_{red1} state but not the $g_{av} = 1.86$ signal that derives from the C_{red2} state. Cluster C appears to exhibit a pentacoordinate iron subsite similar to the one present in the active $[Fe_4S_4]$ form of aconitase (Hu *et al.* 1996). Since Ni is part of cluster C (Qiu *et al.*, 1995), and the $[Fe_4S_4]$ cluster exists in the 2+ and 1+ redox states, the most likely redox state of Ni is Ni(II) in both C_{ox} and C_{red1} states.

Cluster B is a ferredoxin-type $[Fe_4S_4]$ cluster that is diamagnetic when oxidized and paramagnetic with a net spin of $^1/_2$ when reduced ($E^{\circ\prime} = -440$ mV vs NHE). The g values of the reduced state of cluster B, known as B_{red}, are 2.04, 1.94, and 1.90 ($g_{av} = 1.96$) (Lindahl & Ragsdale, 1990a; Lindahl *et al.*, 1990b). This signal reaches a maximum spin intensity of 0.60−0.70 spin per CODH/ACS dimer. The proposed function of this cluster is to transfer electrons from cluster C to external redox mediators, such as ferredoxin (Fd) (Kumar *et al.*, 1993).

The α subunit appears to contain the active site of acetyl-CoA synthesis. It has been isolated and shown to contain 1 Ni and 4 Fe atoms (Xia *et al.*, 1995) in a cluster that presumably is the decomposition product of cluster A. Cluster A is a novel Ni−FeS cluster that is the active site of acetyl-CoA synthesis from CoA, a methylated corrinoid protein, and CO. It has been extensively probed by electron paramagnetic resonance (EPR) (Ragsdale *et al.*, 1982, 1985), electron nuclear double resonance (ENDOR) (Fan *et al.*, 1991), infrared (Ragsdale & Kumar, 1992), Resonance Raman (Qiu *et al.*, 1994, 1995), and Mössbauer spectroscopies (Lindahl *et al.*, 1990b; Hu *et al.*, 1996). On the basis of these spectroscopic studies, a structure consisting of a Ni(II) ion bridged to a $[Fe_4S_4]$ cluster was formulated (Lindahl *et al.*, 1990b; Fan *et al.*, 1991).

Previous studies of CO oxidation by the Ni-containing *C. thermoaceticum* CODH/ACS indicated that this reaction occurs through a ping-pong mechanism that can be divided into two half-reactions (Thauer *et al.*, 1974; Diekert & Thauer, 1978; Kumar *et al.*, 1993; Seravalli *et al.*, 1995). The first half of the reaction is CO oxidation to CO_2, which is associated with reduction of the enzyme; the second is the reoxidation of the enzyme by an external electron acceptor. Pre-steady-state kinetic studies established that there are two distinctive changes in the EPR spectrum associated with the first reductive half-reaction. First, cluster C undergoes conversion from the C_{red1} state to the C_{red2} state, and then, cluster B undergoes reduction (Kumar *et al.*, 1993). Resonance Raman and infrared spectroscopic studies of the cyanide adduct of cluster C (Qiu, *et al.*, 1996), a selective inhibitor of CO oxidation, indicated that this reaction involves a bimetallic mechanism in which water or hydroxide binds to the Ni subsite and CO binds to the $[Fe_4S_4]$ subsite of cluster C. A similar mechanism has been proposed in which the roles of the metals are reversed (Hu *et al.*, 1996). On the basis of steady-state kinetic investigations (Seravalli *et al.*, 1995) and spectroscopic studies (Qiu *et al.*, 1996), an outline of the first half-reaction was developed that included (i) binding of water and CO to the C_{red1} form, (ii) deprotonation of enzyme-bound water to yield enzyme-bound hydroxyl, (iii) nucleophilic attack on coordinated CO by the hydroxyl group to form an enzyme-bound carboxyl or carbohydroxy species, (iv) deprotonation and decarboxylation to form CO_2 and the reduced form of cluster C, and (v) reduction of cluster B by cluster C. The second half-reaction completes the catalytic cycle by reoxidizing cluster B.

There are several gaps in our understanding of the CO oxidation mechanism. Although the conversion of C_{red1} to C_{red2} and the reduction of cluster B have been shown to be kinetically competent (Kumar *et al.*, 1993), the intermediate steps in the catalytic cycle have not been defined. It is not known if the C_{red1} and C_{red2} states are isoelectronic or if C_{red2} is two electrons more reduced than C_{red1}, as recently proposed (Anderson & Lindahl, 1994, 1996). Furthermore, CO oxidation involves two electrons, yet cluster B, which accepts electrons from cluster C, is a typical $[Fe_4S_4]^{2+/1+}$ cluster (Lindahl *et al.*, 1990a,b) that can accept only one electron. This problem has led others (Anderson & Lindahl, 1996) to suggest that there is a redox site called X that accepts the second electron from cluster C. Although reduction of cluster B by cluster C is incorporated as step v (above), the reconversion of C_{red2} to either C_{red1} or C_{ox} has never been observed as a step in catalysis, indicating that the C_{red2} state may be a product state, rather than a transient intermediate, in the reaction. The studies reported here were designed to answer some of these questions. On the basis of the titrations of CODH/ACS with dithionite and CO and pre-steady-state kinetic measurements, we have derived a mechanism to describe the first half-reaction of CO oxidation, and we obtained the values of the microscopic rate constants for each of these steps. Our results suggest that, during pre-steady state, 2 equiv of CO (four electrons) per cluster C are required to reduce clusters B and C. Two electrons are used to rapidly convert C_{red1} to C_{red2} and two more electrons are used to reduce cluster B and center X, a center whose existence can only be inferred. Reduction of cluster B and center X are the rate-limiting steps of the first half-reaction of CO oxidation, while electron transfer to external electron acceptors is rate-limiting during steady-state oxidation of CO.

MATERIALS AND METHODS

Materials. CO (99.9%), N_2 (99.9%) and CO/N_2 mixtures were obtained from Linweld (Lincoln, NE). N_2 was further purified by passage through a heated column of BASF catalyst. Sodium dithionite, potassium ferricyanide, and Trizma base were obtained from Sigma Co., St. Louis, MO. All other materials were of the highest purity available.

Growth of Organism and Protein Purification. C. thermoaceticum strain ATCC 39073 was grown on glucose and CO_2 as previously described (Andreesen *et al.*, 1973). CODH/ACS was purified as previously described (Ragsdale *et al.*, 1983) without the ammonium sulfate precipitation step. All purification operations were performed in an anaerobic chamber from Vacuum Atmospheres, Hawthorne, CA, at 15−20 °C and below 1 ppm of oxygen (Teledyne oxygen analyzer). The specific activity of CODH/ACS ranged from 350 to 450 units mg^{-1}, with 1 unit defined as 1 μmol of CO oxidized min^{-1} at 55 °C using an assay mixture that contained 10 mM methyl viologen, 2 mM dithiothreitol (DTT), and 50 mM Tris-HCl buffer, pH 7.60 (Ragsdale *et al.*, 1983). Protein concentrations were determined by the rose bengal dye-binding assay (Elliott & Brewer, 1978). Protein was judged more than 95% pure by SDS−PAGE using Coomassie brilliant blue for staining. Samples of CODH/ACS for stopped-flow and EPR titrations were freed of DTT and other reductants by extensive dialysis with reductant-free buffers in Microcon-30 concentrators.

Reductive CODH/ACS Titrations with Dithionite and CO. Samples for titrations were prepared in 1 mL glass V-vials (Wheaton, Milville, NJ) inside the anaerobic chamber. To eliminate loss of reducing equivalents by traces of oxygen, all buffers contained 500 μM protocatechuic acid (PCA, 3,4-dihydroxybenzoic acid) and 0.18 unit/mL of protocatechuic acid dioxygenase (PCD, generous gifts from Drs. David Ballou and John Lipscomb). This reaction proceeds by a ternary complex (PCD−PCA−O_2) mechanism without release of electrons (Valentine, 1994), and thus, it does not affect the concentration of reducing equivalents. After the reaction vials were sealed, aliquots of freshly prepared sodium dithionite (10 mM) or CO stock solutions (970 μM at 25 °C) were added to start the reactions. Samples titrated with dithionite were incubated for 1 h, while those reacted with CO were incubated for 20−30 min.[2] Samples were then transferred into standard X-band quartz EPR tubes and immediately frozen in liquid nitrogen. Dithionite stock solutions (~1.1 M) were prepared in 0.2 M NaOH, diluted 100-fold, and standardized against potassium ferricyanide, flavin mononucleotide (FMN), and methyl viologen before and after the experiments. The concentration was found to change by less than 1% after 1 day. All concentrations of CODH/ACS in this paper refer to the $\alpha\beta$ dimeric form that contains one each of clusters A, B, and C. Since dithionite and CO are two-electron reductants, their concentrations as reducing equivalents are equal to twice their molar mass concentrations.

The concentration of B_{red} was obtained by doubly integrating the $g_{av} = 1.94$ EPR signal at 30 K, while the concentrations of the C_{red1} and C_{red2} forms of cluster C were obtained by subtracting the double integration for B_{red} at 30 K from the double integration at 10 K. This is an accurate measurement of the spin quantitation of cluster C since its EPR signal is absent above 20 K due to relaxation broadening.

The relaxation properties of C_{red1} and C_{red2} are too similar to use temperature changes to distinguish them, so the following method was used. The EPR spectrum of a CODH/ACS sample showing only the C_{red1} signal was recorded and used as reference. This spectrum was multiplied by a variable fraction and subtracted from the spectrum of samples containing both C_{red1} and C_{red2} to calculate the amount of C_{red1} present. After subtraction, the resulting spectrum contained only the signals for B_{red} and C_{red2}. The integration for the B_{red} signal (performed at 30 K) was subtracted from that of the total spectrum to quantitate the intensity of the C_{red2} signal.

Optical titrations were carried out in a 3 mL Pyrex cuvette (Spectrocell, Skokie, IL) modified at the top to fit a 20 mm black butyl rubber anaerobic stopper. Additions were made using gastight Hamilton syringes. Titrations were performed at 25 °C in buffers containing 50 mM Tris, pH 7.60, with PCA and PCD. Optical titrations were monitored at 420 nm in a Cary-14 spectrophotometer modified by Olis (Bogart, GA).

EPR Spectroscopy. EPR spectra were recorded on a Bruker ESP 300e spectrometer equipped with an Oxford ITC4 cryostat and temperature controller, a Hewlett-Packard 5340A frequency counter, and a Bruker ER 035M gaussmeter. Spin concentrations were measured by comparing the double integrals of the spectra with a 1.0 mM copper perchlorate standard using software provided by Bruker.

Rapid Kinetic Experiments. Anaerobic solutions for stopped-flow kinetics were prepared in 50 mM Tris-HCl buffer, pH 7.60, in the presence of PCA and PCD or, for rapid freeze−quench EPR kinetics (FQ-EPR), in 50 mM Tris buffer, pH 7.60, with 2.0 mM DTT in the anaerobic chamber. The solutions were transferred into anaerobic tonometers that served as reservoirs for the drive syringes. CO was added by bubbling with CO/N_2 gas mixtures that afforded, after mixing in the stopped-flow apparatus, final CO concentrations of 4.85, 48.5, 97, 146, 242, and 485 μM. An Applied Photophysics (Leatherhead, U.K.) Model DX.17MV spectrophotometer/spectrofluorometer, connected to a nitrogen-bubbled anaerobic water circulation bath, was employed for stopped-flow experiments. FQ-EPR experiments were carried out as described before (Kumar *et al.*, 1993) using a Model 745 syringe-ram controller from Update Instruments, Inc. (Madison, WI).

Simulation of Stopped-Flow and Freeze−Quench Data. Kinetic traces of absorbance or spin intensity vs time were simulated using the DOS/Windows 3.1 version of the program package KINSIM/FITSIM from Washington University, St. Louis, MO (Zimmerle & Frieden, 1989, Barshop *et al.*, 1983) and modified by Gary Xin Hua and Dr. Bryce Plapp of the University of Iowa. Data were first fitted to a single-exponential equation to calculate response factors for the corresponding intensities of the cluster B and cluster C EPR signals. Changes in extinction coefficients were calculated for stopped-flow traces from the fitted exponential-

[2] In order to ensure that all electrons from dithionite were available as reducing equivalents, samples of FdII from *C. thermoaceticum* (which has an $E^{\circ\prime} = -440$ mV and two $[Fe_4S_4]$ clusters per molecule) were titrated and followed by EPR and UV−visible spectroscopies. Both titrations (not shown) required 1.0−1.2 mol of dithionite/mol of ferredoxin or 1 electron per $[Fe_4S_4]^{2+}$. The maximal spin intensity was 1.9 spin per ferredoxin while the slope of the absorption changes at 420 nm vs dithionite concentration was 10.5 mM^{-1} cm^{-1}.

decay amplitudes at 420 nm using the software from Applied Photophysics. The initial CO and CODH/ACS concentrations that were used in the KINSIM program were in micromolar concentration units, the simulations were carried out using the flux tolerance method, and rate constants were fitted using the Marquardt algorithm. The final simulated data generated by KINSIM and FITSIM were plotted using SigmaPlot (Jandel Scientific, San Rafael, CA).

Steady-State Measurements. The values of k_{cat} and k_{cat}/K_m for CO with methyl viologen as electron acceptor are the same as reported earlier [Figure 8 in Seravalli *et al.* (1995)]. The steady-state reduction rates of FdII from *C. thermoaceticum* by CO were monitored at 420 nm in 50 mM Tris buffer, pH 7.60, containing saturating concentrations of CO (970 μM) at 25 °C, 2−10 nM CODH/ACS, and variable FdII concentrations. Initial rates were plotted versus FdII concentration to obtain values of k_{cat} and K_m for FdII.

RESULTS

Dithionite Titration of CODH/ACS. CODH/ACS, which was free of dithionite, was incubated in PCA/PCD-containing buffers at pH 7.60 to ensure that the solutions remained O_2-free during titrations. After the sample was frozen in liquid nitrogen, the EPR signals for C_{red1} with g values of 2.01, 1.81, and 1.65 (0.25 spin per $\alpha\beta$ CODH/ACS dimer) and B_{red} with g values of 2.04, 1.94, and 1.89 (0.18 spin per CODH/ACS dimer) were observed at 10 K (Figure 1). These samples were incubated for 60 min; longer incubations did not change the spectra. As the samples were titrated with increasing concentrations of sodium dithionite, the signal intensity of B_{red} increased (●, Figure 1B) to a maximum of 0.6 spin per CODH/ACS dimer. The initial slope of the B_{red} titration was 0.93 spin per equiv of dithionite, and the titration leveled off between 0.5 and 1.0 equiv of dithionite per CODH/ACS dimer. At 30 K (not shown) only the B_{red} signals were observed; the signals for cluster C were not detected due to relaxation broadening. The intensity of the C_{red1} signal (○, Figure 1B) at 10 K showed a slight increase to a maximum of 0.35 ± 0.03 spin of C_{red1} per CODH/ACS dimer. None of these samples exhibited the NiFeC or the C_{red2} signals. Therefore, 1 equiv of dithionite (2 electrons) reduced B_{ox} to B_{red} by 0.40 spin per CODH/ACS dimer and C_{ox} to C_{red1} by 0.10 spin per CODH/ACS dimer. Considering the slope from the early phase of the titration, two electrons per cluster B were required to reduce B_{ox} to B_{red} by one electron.

A similar titration by UV−visible spectroscopy was performed in order to monitor reduction of the clusters. Addition of 1 equiv of dithionite per CODH/ACS dimer resulted in a slope of absorption decrease at 420 nm vs dithionite concentration of 8.0 mM^{-1} cm^{-1} (not shown). Such an extinction coefficient change is typical of the reduction of one $[Fe_4S_4]^{2+}$ cluster to the $[Fe_4S_4]^{+}$ state and confirmed the EPR results showing that two electrons were required per cluster B for reduction from B_{ox} to B_{red}. These combined results, therefore, indicate that an EPR-silent electron acceptor must exist in CODH/ACS that can accept 50% of the electrons required to reduce cluster B.

CO Titration of CODH/ACS. A second CODH/ACS sample that was free of reductants but contained PCA/PCD showed 0.22 spin of B_{red} per CODH/ACS dimer and 0.25 spins of the C_{red1} signal per CODH/ACS dimer. As aliquots of a CO-saturated buffer solution were added, the intensity of B_{red} increased (●, Figure 2B) to a maximum of 0.65 spin per CODH/ACS dimer. The C_{red1} intensity increased slightly to 0.35−0.40 spin per CODH/ACS dimer (○, Figure 2B) within the range of CO required to titrate cluster B. The initial slope of the cluster B titration was 0.91 spin per mol of CO (2.2 electrons per spin). Another EPR titration at pH 9.1 using CO as reductant (with a redox potential ∼ −640 mV) gave identical results as at pH 7.60 (redox potential ∼ 550 mV), suggesting that lack of reducing power was not

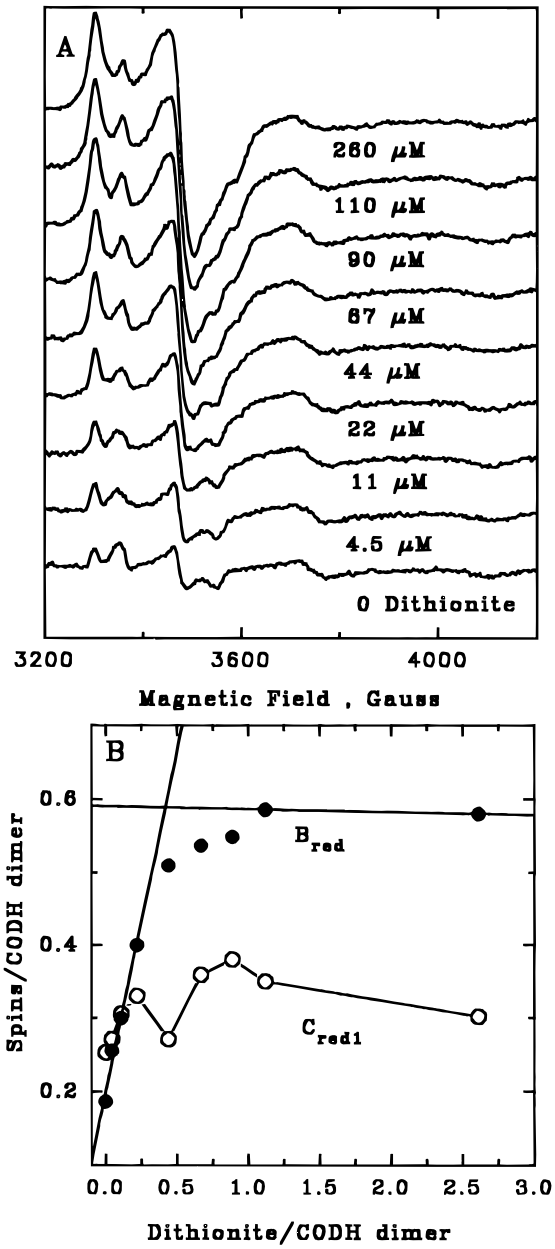

FIGURE 1: (A) Titration of CODH/ACS with dithionite. CODH/ACS (100 μM in $\alpha\beta$ dimers) was equilibrated with the indicated concentration of sodium dithionite at 18 °C for 60−70 min. Samples were frozen in liquid nitrogen and EPR spectra were recorded. Spectroscopic parameters: temperature, 10 K; microwave frequency, 9.44−9.43 GHz; microwave power, 0.040 mW; receiver gain, 40 000; modulation frequency, 100 kHz; modulation amplitude, 10 G. (B) Dependence of the integrated intensity of B_{red} at 30 K and C_{red1} at 10 K on the amount of dithionite added per CODH/ACS dimer. The integrated intensity of C_{red1} was obtained by subtraction of the integrated intensity of B_{red} at 30 K from the total integrated intensity at 10 K.

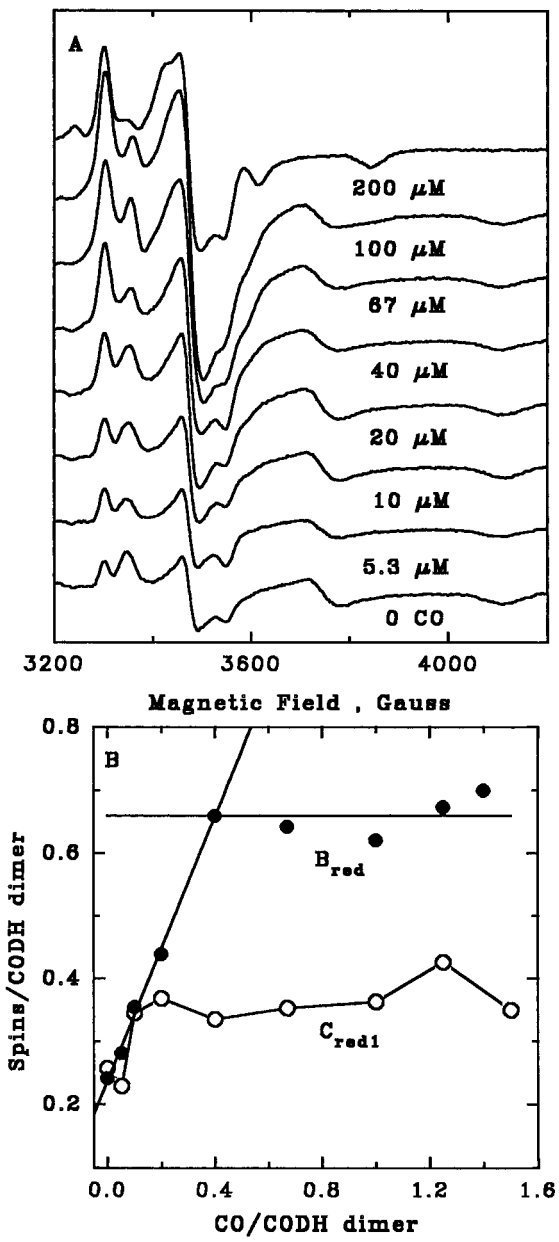

FIGURE 2: (A) Titration of CODH/ACS with CO. CODH/ACS (100 μM dimer) was equilibrated with the indicated concentration of CO at 18 °C for 15−20 min and the samples were then frozen in liquid nitrogen. EPR conditions were the same as in Figure 1A except that the microwave power was 0.160 mW and the receiver gain was 20 000. (B) Dependence of the integrated intensities of B_{red} and C_{red1} at 10 K on the amount of CO added per CODH/ACS dimer.

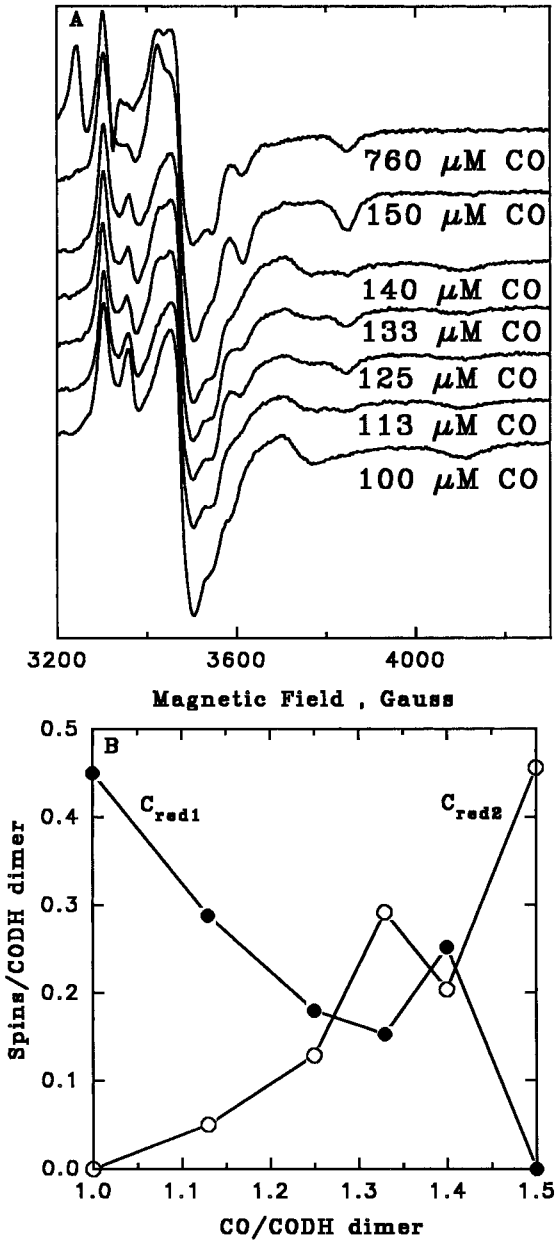

FIGURE 3: (A) Titration of CODH/ACS with 1.0−1.5 equivalents of CO per CODH. CODH/ACS (100 μM in $\alpha\beta$ dimers) was equilibrated with the indicated CO concentrations at 18 °C for 20−30 min. Samples were frozen in liquid nitrogen and EPR spectra were recorded using the same parameters as in Figure 1A except that the microwave power was 0.160 mW and the receiver gain was 50 000. (B) Dependence of the integrated intensities of C_{red1} and C_{red2} on the amount of CO added per CODH/ACS dimer. The concentrations of C_{red1} and C_{red2} were calculated as described in Materials and Methods.

the reason for the requirement of 1 mol of CO (two electrons) to reduce 1 mol of cluster B. Also reactivity is not an issue; the rates of conversion of C_{red1} to C_{red2} and of B_{ox} to B_{red} as followed by FQ-EPR (Kumar *et al.*, 1993) are both faster than k_{cat} (100 s^{-1}). A weak isotropic signal with a *g* value of 4.30 (not shown) was observed in all titration samples. The intensity of this signal (0.3 spin per CODH/ACS dimer) did not change during the CO titration; thus, this signal could not account for missing reducing equivalents in the dithionite or CO titrations. Therefore, as with the dithionite titration, the CO titration experiments indicate that an EPR-silent electron acceptor, termed S, must be present to account for 50% of the electrons required to reduce cluster B.

The CO titration differed in two respects from the dithionite titration. First, as 1.0−2.0 molecules of CO per CODH/ACS dimer were added, the total EPR signal intensity of cluster C remained nearly constant, but the spectrum of C_{red2} replaced that of C_{red1}. To further explore this conversion, we titrated a third CODH/ACS sample with CO concentrations ranging from 100 to 150 μM (1.0−1.5 moles of CO per mol of CODH/ACS dimer). The results shown in Figure 3 indicate that 0.5 mol of CO per CODH/ACS dimer was required to fully convert 0.45 spin of C_{red1} per CODH/ACS dimer (●) to C_{red2} (○), which corresponds to 1.1 mol of CO or 2.2 electrons per C_{red1}. Thus, C_{red2} can be

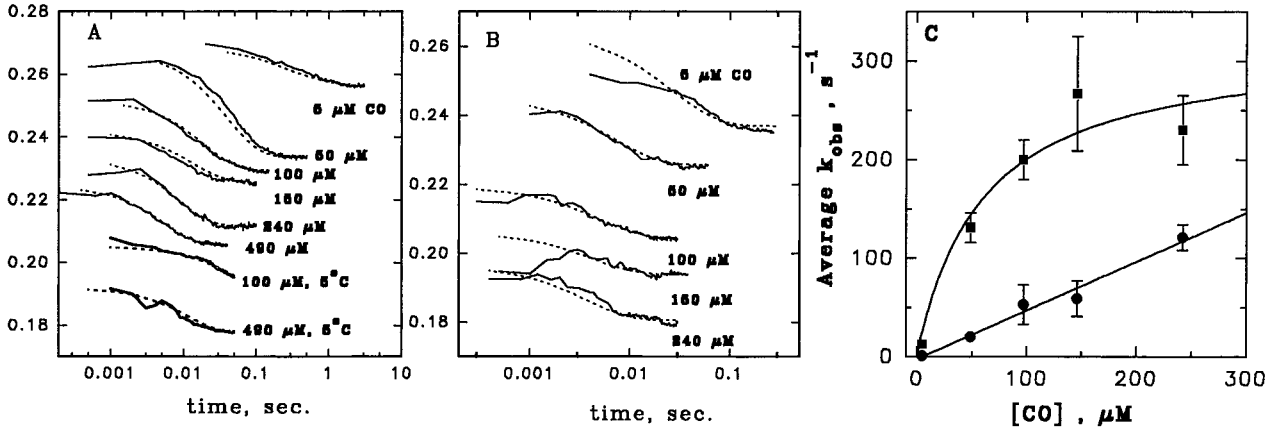

FIGURE 4: Stopped-flow traces and simulated traces of CODH/ACS reduction monitored at 420 nm. The micromolar CO concentrations are shown on the figure. Simulations were performed as described in Materials and Methods using the mechanism described by Scheme 1 and the rate constants given in Table 1. Individual traces are shown shifted along the absorbance axis for clarity. (A) CODH/ACS (7.7 μM $\alpha\beta$ dimers at 10 °C and 10 μM $\alpha\beta$ dimers at 5 °C final concentrations) and CO were rapidly mixed in the stopped-flow apparatus at 10 °C (top six traces) and at 5 °C (bottom two traces) at the indicated final CO concentrations. (B) CODH/ACS (6.0 μM $\alpha\beta$ dimers final concentration) was rapidly mixed in the stopped-flow apparatus at 25 °C with CO at the indicated final concentrations. (C) Dependence of the average value of k_{obs} from panels A and B on the final CO concentration at 25 °C (■) and at 10 °C (●). Error bars are the standard deviations from at least 5 determinations.

either a C_{red1}−CO complex or, as previously proposed (Anderson & Lindahl, 1994), the product of a two-electron reduction of C_{red1}. The total integration for cluster C for this sample (0.45 spin per CODH/ACS dimer) did not change during the titration, indicating that an EPR-silent intermediate state between C_{red1} and C_{red2} did not accumulate. The second feature of the CO titration that was different from the dithionite titration was that when the enzyme was equilibrated with more than 2 equiv of CO per CODH/ACS dimer, the NiFeC signal from cluster A was formed (top spectrum in Figure 3A).

Stopped-Flow Studies of the Reaction of CODH/ACS with CO. We had previously monitored the reduction of the CODH/ACS clusters at 420 nm and 5 °C using stopped-flow kinetics in solutions containing 10% CO (97 μM final CO concentration) (Kumar *et al.*, 1993). In the work described here, we performed stopped-flow studies at 50% CO (485 μM CO) at 5 °C and a wide range of CO concentrations at 10 °C and 25 °C. Figure 4A,B shows representative kinetic traces obtained by following the reduction of CODH/ACS by CO at 420 nm. The average values of k_{obs} from at least 5 experiments were then plotted vs the CO concentration (Figure 4C). Table 1 shows the parameters for the linear fit for the 10 °C data and the hyperbolic fit for the 25 °C data. Under all conditions, the values of k_{max}/K_d (slope of k_{obs} vs CO concentration) derived from stopped-flow experiments were greater than the values of $(k_{cat}/K_m)_{CO}$ obtained from the steady-state data (Seravalli *et al.*, 1995), and the k_{max} values from stopped-flow experiments were greater than the $(k_{cat})_{CO}$ values from the steady-state data. The dotted lines shown in Figure 4 were obtained by kinetic simulation methods described below.

Simulation of Stopped-Flow and Freeze−Quench Data. Figure 5 shows the results of FQ-EPR studies in which CODH/ACS was rapidly mixed with CO at final concentrations of 97 μM at 5 °C, 240 μM at 5 °C, or 485 μM at 25 °C. The rate of reduction of the CODH/ACS clusters followed by optical absorption at 420 nm is similar to the EPR-monitored rate of reduction of cluster B; however, this rate is 3−8-fold smaller than the conversion of C_{red1} to C_{red2}, which has k_{obs} values ranging between 300 and 1000 s^{-1}.

Table 1: Parameters from Stopped-Flow and Steady-State Experiments

	5 °C	10 °C	25 °C
extinction coefficient change[a] (mM^{-1} cm^{-1})	1.40 ± 0.1	3.2 ± 0.9	2.0 ± 0.6
k_{max}/K_d (μM^{-1} s^{-1})	0.19[b]	0.48 ± 0.02[b]	4.5 ± 1.8
k_{max} (s^{-1})	>100	>200	340 ± 70
K_d for CO (μM)	>530	>400	76 ± 30
$(k_{cat}/K_m)_{CO}$[c] (μM^{-1} s^{-1})	0.095 ± 0.010	0.376 ± 0.040	0.86 ± 0.05[d]
k_{catCO}[c] (s^{-1})	10 ± 1	37 ± 3	95 ± 10[d]
K_{mCO} (μM)	106 ± 15	98 ± 14	110 ± 17[d]

[a] Extinction coefficients were calculated from the average amplitudes of the first-exponential decay fits at 420 nm for experiments with excess CO relative to CODH/ACS. [b] Steady-state parameters are taken from Seravalli *et al.* (1995). Methyl viologen (10 mM) was the electron acceptor. [c] At 10 °C, the dependence of k_{obs} on CO is linear, and thus, only k_{cat}/K_d can be calculated. At 5 °C we only have data at 100 and 480 μM CO, and thus, k_{cat}/K_d was calculated from the average k_{obs} at these two concentrations. The lower limits for k_{max} are the observed rates with 485 μM CO. [d] Measured by steady-state reduction of 10 μM CO with 25 μM Fd, pH 7.60, 50 mM Tris, and 2 mM DTT. The K_m for ferredoxin was found to be 8.0 μM.

No changes in the UV−visible absorption spectrum that could be ascribed to cluster C reduction were observed during this time frame (first 10 ms). This indicates that the $[Fe_4S_4]$ moiety of cluster C must remain in the same redox state during the C_{red1} to C_{red2} conversion, since FeS clusters are expected to undergo bleaching when reduced.

A two-step kinetic mechanism, shown by eqs 2 and 3,

$$E + CO \rightleftharpoons E{-}CO \quad (2)$$

$$E{-}CO \rightleftharpoons F + CO_2 \quad (3)$$

was used to fit *separately* the conversion of C_{red1} to C_{red2}. The labels E and F correspond to CODH/ACS with cluster C in the C_{red1} and C_{red2} states, respectively. A similar two-step mechanism, shown by eqs 4 and 5, was used to simulate

$$F + CO \rightleftharpoons F\text{-}CO \quad (4)$$

$$F\text{-}CO \rightleftharpoons G + CO_2 \quad (5)$$

the stopped-flow kinetic data and FQ-EPR data for reduction

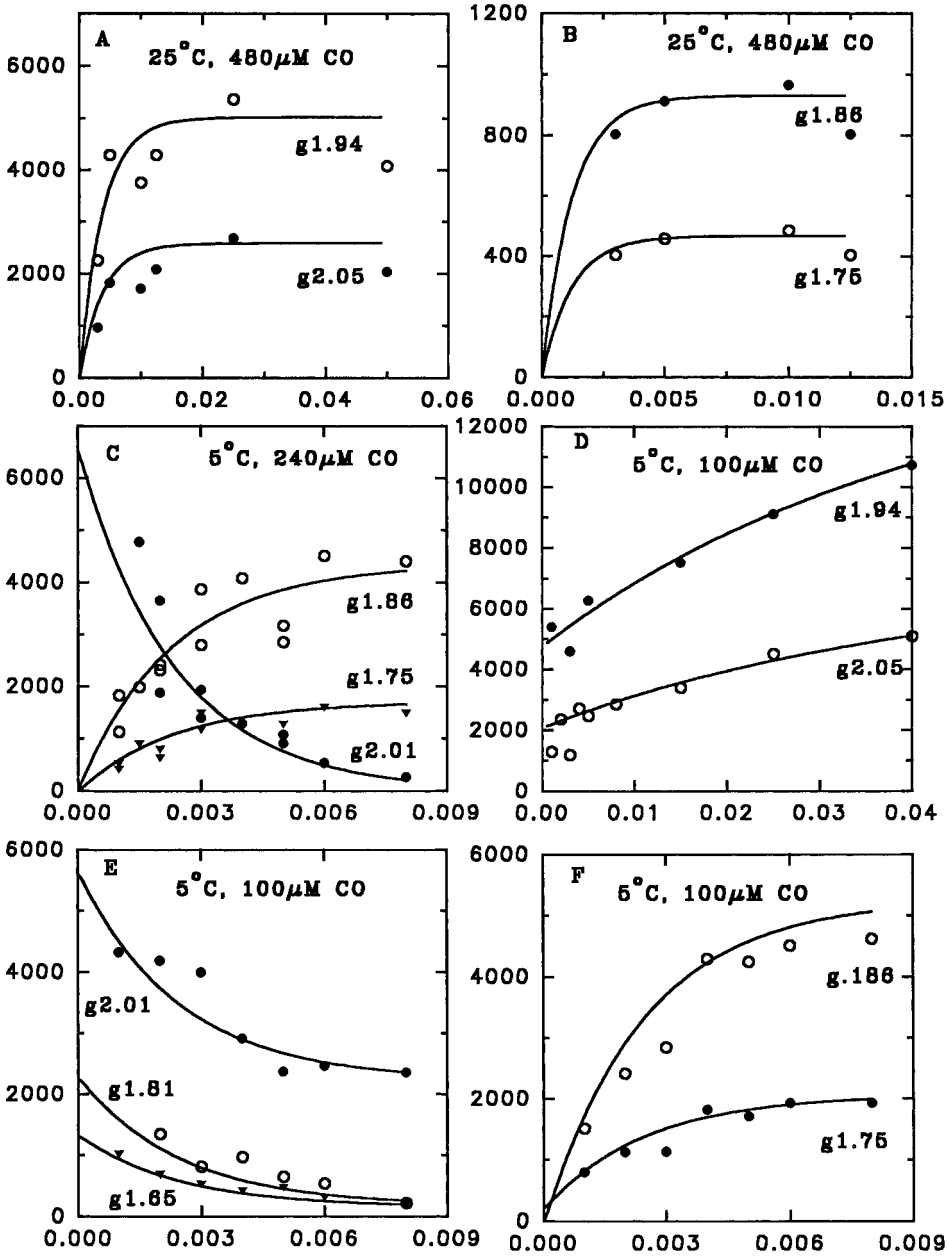

FIGURE 5: Freeze−quench EPR data points and simulated traces. Simulations were performed as described in Materials and Methods using the mechanism in Scheme 1 and rate constants given in Table 1. The *x*-scale is in seconds. Other conditions and final concentrations are as follows: (A, B) 80 μM CODH/ACS $\alpha\beta$ dimers and 480 μM CO at 25 °C; (C) 30 μM CODH/ACS $\alpha\beta$ dimers and 240 μM CO at 5 °C; (D−F) 30 μM CODH/ACS $\alpha\beta$ dimers and 100 μM CO at 5 °C. EPR spectra were recorded as described in Kumar *et al.* (1993). Intensities for each of the *g* values were directly read from the EPR spectra at a given delay time shown in seconds.

of cluster B (*g* values 1.94 and 2.05). The labels F and G correspond to CODH/ACS with cluster B in the B_{ox} and B_{red} states, respectively. Two steps are required to account for the hyperbolic dependence of the stopped-flow rates on CO concentration at 25 °C, shown in Figure 4C. Since both the reduction of C_{red1} to C_{red2} and that of B_{ox} to B_{red} are two-electron processes, a total of four steps were required to fit all the data shown in Figures 4 and 5. The fitted rate constants, shown in Table 2, clearly indicate that the EPR changes for cluster C are faster than the EPR and UV−visible absorption changes for cluster B. Therefore the first step in the mechanism must correspond to binding of CO to C_{red1}; the second step is then the reduction of C_{red1} into C_{red2}; the third step is binding of a second equivalent of CO; and the fourth step is reduction of cluster B. Our final kinetic mechanism is described by Scheme 1, in which the redox states of clusters B and C and center X are indicated. The rationale for Scheme 1 is described below.

DISCUSSION

EPR Titration of CODH/ACS. CODH/ACS from *C. thermoaceticum* contains three redox-active clusters. How the electrons are distributed among these clusters has been studied here and in earlier investigations by our and Lindahl's group. In the studies reported here, we performed similar equilibrium redox titrations with dithionite and CO; under these conditions, the redox reactions are under thermodynamic control. We also performed rapid mixing experiments to follow the flow of electrons from CO to the different redox sites in the enzyme; under these conditions, the reaction is under kinetic control and the rate of electron transfer can be related to the rate at which the enzyme oxidizes CO to CO_2.

Table 2: Summary of Microscopic Rate Constants

process	rate constant[a]	5 °C	10 °C	25 °C
$C_{red1} + CO \rightarrow C_{red1}-CO$	k_1 (μM^{-1} s^{-1})	240 ± 110		300 ± 60
$C_{red1}CO \rightarrow C_{red1} + CO$	k_{-1} (s^{-1})	1510 ± 460		480 ± 100
$C_{red1}-CO \rightarrow C_{red2} + CO2$	k_2 (s^{-1})	450 ± 14		810 ± 100
$C_{red2} + CO_2 \rightarrow C_{red1}-CO$	k_{-2} (μM^{-1} s^{-1})	0.0 ± 0.1		0.017 ± 0.003
$C_{red2} + CO \rightarrow C_{red2}-CO$	k_3 (μM^{-1} s^{-1})	4.4 ± 0.5	5.0 ± 0.4	20 ± 2
$C_{red2}-CO \rightarrow C_{red2}+ CO$	k_{-3} (s^{-1})	2000 ± 210	3600 ± 280	2800 ± 270
$C_{red2}-CO$, $B_{ox} \rightarrow C_{red2}$, $B_{red} + CO_2$	k_4 (s^{-1})	132 ± 6	480 ± 30	500 ± 60
C_{red2}, $B_{red} + CO_2 \rightarrow C_{red2}-CO$, B_{ox}	k_{-4} (μM^{-1} s^{-1})	0.045 ± 0.02	0.030 ± 0.005	0.13 ± 0.02
$C_{red1}-CO \rightleftharpoons C_{red1} + CO$	K_{d1} (μM)	6.3 ± 3.5		1.6 ± 0.5
$C_{red2}-CO \rightleftharpoons C_{red2} + CO$	K_{d3} (μM)	450 ± 70	720 ± 80	140
	k_2/K_{d1} (μM^{-1} s^{-1})	70 ± 39		500 ± 160
	k_4/K_{d3} (μM^{-1} s^{-1})	0.29 ± 0.05	0.67 ± 0.08	3.6 ± 0.7

[a] Mechanism equations are explained in the text and in Scheme 1. [b] FQ-EPR were carried out at 5 and 25 °C. Upper limits for second-order steps were set at 1000 μM^{-1} s^{-1} and for first-order steps were 1×10^{13} s^{-1}.

Scheme 1

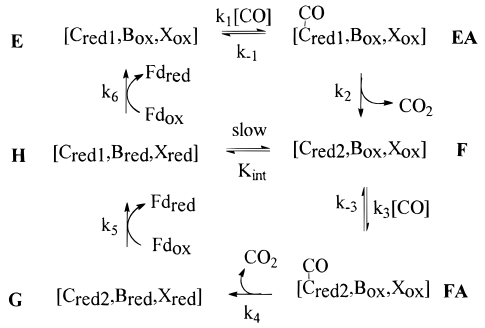

Both the static titrations and the rapid mixing experiments were followed by EPR and by UV−visible spectroscopy.

When Lindahl and co-workers performed redox titrations of CODH/ACS with CO and sodium dithionite, they found that four electrons per CODH/ACS dimer elicited 90% of the observed optical absorption changes (Shin *et al.*, 1992) and concluded that two electrons were involved in reducing two $[Fe_4S_4]^{2+}$ clusters and two electrons reduced other spectroscopically silent one-electron redox sites. Subsequently, on the basis of CO titrations, Anderson and Lindahl (1996) proposed that four electrons from 2 mol of CO reduce cluster C from the C_{red1} state by two electrons to form C_{red2}, reduce cluster B by one electron, and reduce a new center X by one electron. Thus, the C_{red2} state was argued to be two electrons more reduced than the C_{red1} state.

The results of the static CO and dithionite titrations described here are in overall agreement with the conclusions of Anderson and Lindahl (1996). We found that 2 electron equivalents per cluster B were required to reduce B_{ox} to the B_{red} state. Since this is a one-electron reduction, there must be another one-electron acceptor (presumably the center X described above) present in CODH/ACS. Center X must have a redox potential that is similar to that of cluster B (-380 mV $> E^{\circ\prime} > -500$ mV), since it accounts for 50% of the reducing equivalents taken up (Figures 1 and 2). All of the EPR or UV−visible spectroscopic changes observed during the dithionite titration of cluster B could be ascribed to cluster B reduction. Therefore, cluster X must be EPR- and UV−visible-silent. A paramagnetic state of cluster A has never been observed as a result of reaction with dithionite, and cluster C reacts only very slowly with much higher than stoichiometric concentrations of dithionite. However, clusters B and C undergo spectroscopic changes upon reaction with low concentrations of CO and cluster A at high concentrations. The equilibrium titrations with CO indicate that C_{red2} must be two electrons more reduced than C_{red1} since the conversion of C_{red1} to C_{red2} required two electrons (1 mol of CO). This conclusion was reinforced by rapid kinetic experiments that are discussed below. The other possible conclusion that C_{red2} might be a CO-bound form of C_{red1} (i.e., $C_{red1}-CO$) and isoelectronic with C_{red1} was not supported by the rapid kinetics experiments.

Simulation of Pre-Steady-State Kinetics. The equilibrium redox titrations served as a background for rapid kinetic studies, which were carried out to identify the steps involved in CO oxidation. Preliminary FQ-EPR studies had shown that the first EPR-detectable event that occurred when CODH/ACS in the C_{red1} form was reacted with CO was the conversion of C_{red1} to C_{red2} (Kumar *et al.*, 1993). Next, cluster B underwent conversion to the paramagnetic B_{red} state at a rate that was 4−6 times slower than the rate of C_{red2} formation. Both of these steps were found to be kinetically competent for CO oxidation to CO_2 and supported a model that was proposed to explain the mechanism (Kumar *et al.*, 1993). This model (model A) included CO binding to cluster C, followed by reduction of cluster C as CO_2 is formed, electron transfer to cluster B, and finally transfer of electrons from cluster B to external acceptors. One problem with this model is immediately obvious. Cluster B is a $[Fe_4S_4]^{2+/1+}$ cluster that can only accept one electron.[3] One way to solve this quandary is to include a one-electron acceptor, X, in the mechanism as was done by Anderson and Lindahl (1996), who proposed a model (model B), comprising eqs 6−8. In

$$[C_{red1}] + CO + H_2O \rightleftharpoons [C_{red2}] + CO_2 + 2\,H^+ \quad (6)$$

$$[C_{red2}] + B_{ox} \rightleftharpoons [C_{int}] + B_{red} \quad (7)$$

$$[C_{int}] + X_{ox} \rightleftharpoons [C_{red1}] + X_{red} \quad (8)$$

this model, cluster C cycles between three redox states, C_{red1},

[3] Calculation of integrated intensities for FQ-EPR data points was performed by the following method. After fitting the traces in Figure 5 to single exponentials, we measured the total intensity change for the $g = 1.65$ (C_{red1}), the $g = 1.75$ (C_{red2}), and the $g = 1.94$ (B_{red}) signals and calculated the *ratio* of the intensities of cluster C (sum of C_{red1} and C_{red2}) to cluster B. These results showed that 0.3 spin per CODH/ACS dimer of C_{red1} underwent conversion to 0.3 spin of C_{red2} and 0.3 spin of B_{red}, i.e., a 1:1 ratio of C_{red2} to B_{red}. This observation requires the inclusion of X_{ox} in the mechanism. A similar conclusion was reached by similar measurement of the amplitudes of stopped-flow changes. Thus, during CO oxidation, the enzyme undergoes two turnovers to completely reduce C_{red1} and partially reduce B_{ox}.

C_{int}, and C_{red2}, which differ in redox state by one electron. C_{red1} was proposed to be a Ni^{2+} center coupled to a $[Fe_4S_4]^{1+}$ cluster, whereas C_{red2} was proposed to contain Ni^{1+}, the cluster in the 1+ state, and a one-electron-reduced Ni ligand. C_{red1} was proposed to bind CO to form C_{red2} and CO_2. Then, reduction of cluster B by C_{red2} (eq 7) was proposed to yield an EPR-silent C_{int} state that returns to the C_{red1} form by reducing center X. B_{red} or X_{red} was proposed to reduce external electron acceptors.

Since models A and B invoke EPR spectral changes in clusters B and C during the catalytic cycle, all of the elementary steps in the CO oxidation mechanism could potentially be identified and their rates of formation and decay could be measured by FQ-EPR. However, since FQ-EPR is a discontinuous method and requires large amounts of enzyme, the precision by which rate constants can be measured is limited by the number of samples that can be analyzed. Other problems with obtaining highly quantitative FQ-EPR kinetic data relate to the method of FQ-EPR sample preparation. A small variation in packing density from sample to sample and a slightly variable amount of frozen isopentane that is incorporated into each sample lead to variations in EPR signal intensities. On the other hand, the stopped-flow method is continuous and allows 1000 data points to be collected in a single experiment. Thus, highly accurate rate constants can be measured for processes that result in optical spectroscopic changes, such as cluster B oxidation and reduction. However, some of the steps of CO oxidation (such as cluster C redox changes and substrate binding) cannot be followed by stopped-flow spectroscopy because they do not result in a change in the optical spectrum. Therefore, stopped-flow spectroscopic studies were used to augment the FQ-EPR studies.

Models A and B described above served as the preliminary mechanistic models. The first step one observes when CODH/ACS is reacted with CO is the conversion of C_{red1} to the C_{red2} state. The mechanistic restrictions of this step could be established by fitting and simulating the FQ-EPR data at 5 °C obtained with varying initial CO concentrations. A one-step process (e.g., model B) failed to fit the traces for decay of C_{red1} and formation of C_{red2}, yielding error limits in the rate constants that were higher than 100%. In addition, the mean square standard deviation of the data from the fit to a one-step mechanism was 2-fold higher and the standard error was 8-fold worse than those parameters for a two-step mechanism. Therefore, model C was developed, which includes two steps responsible for the observed changes in the spectral properties of cluster C. First, C_{red1} reacts with CO to form a $C_{red1}-CO$ complex; then, $C_{red1}-CO$ converts to C_{red2} as CO_2 is formed. These two steps constitute the first two steps in Scheme 1 with rate constants defined in Table 2. The second step must be irreversible ($k_{-2} = 0\ \mu M^{-1}\ s^{-1}$) because the EPR spectrum of C_{red1} completely disappeared (Figure 5C,E) upon conversion to C_{red2}. This model implies, as proposed earlier (Anderson & Lindahl, 1994), that departure of CO_2 produces a form of cluster C that is two electrons more reduced than C_{red1}.

The next EPR-detectable step in CO oxidation involves the reduction of cluster B. Since this step is accompanied by bleaching of the FeS cluster absorption band and generation of a characteristic $[Fe_4S_4]^{1+}$ EPR spectrum, it could be analyzed by FQ-EPR and stopped-flow kinetics. The amplitudes of the FQ-EPR and stopped-flow changes demonstrated that only one cluster B is reduced per C_{red2} formed.[3,4] It was necessary to include the one-electron acceptor (X_{ox}) in the mechanism to account for the reduction of cluster B, which is a one-electron acceptor (rationalized above). We have not been able to detect any spectral changes associated with the decay of X_{ox} or the formation of X_{red}. Reduction of cluster B and of X_{ox} by internal electron transfer from C_{red2}, as it is oxidized to C_{red1}, could involve one or two steps and could involve the intermediacy of a C_{int} state (e.g., model B). However, we were unable to obtain satisfactory fits to the FQ-EPR and stopped-flow data using any model that did not include another step of CO binding in the mechanism. Including a second cycle of CO binding as in Scheme 1 greatly improved the fits to the data and yielded excellent simulations of the FQ-EPR and stopped-flow kinetic traces. In addition, the dependencies of the rates of reduction of clusters C and B on the CO concentration strongly supported the requirement for a second CO binding cycle. For example, the value of K_{d1} was ~50-fold lower than K_{d3}, and the reduction of cluster B, as followed by stopped-flow kinetics, yielded K_d values for CO (Figure 4C) that closely agree with the derived K_{d3} values. Furthermore, the observed hyperbolic dependence of k_{obs} for cluster B reduction on CO concentration (at 25 °C) requires a binding step prior to cluster B reduction. In summary, the kinetics of the spectroscopic changes for clusters B and C exhibit distinct CO concentration dependences, requiring two separate cycles of CO oxidation; binding of a second CO molecule must take place *prior* to reduction of cluster B but *after* the first turnover, which reduces C_{red1} to C_{red2}. Therefore, as shown in Scheme 1, our results indicate that the state of cluster C after the first CO turnover is C_{red2}, which binds the second CO molecule to form the $C_{red2}-CO$ complex.[5] The two turnovers of CO oxidation must reduce cluster C by two electrons to form C_{red2} and reduce one cluster B to the B_{red} state and one X_{ox} center to X_{red} by one electron each. Presumably, the two-electron reduction of cluster C_{red1} greatly decreases its affinity for CO.

[4] The optical changes observed for the reaction of CODH/ACS with excess CO shown in Figure 4 yielded extinction coefficients of 2000−3000 $M^{-1}\ cm^{-1}$ at 420 nm. These are much smaller than the reported coefficient change of 14 700 $M^{-1}\ s^{-1}$ for extended incubation of CODH/ACS with CO (Shin *et al.*, 1992). We explain the discrepancy as follows. The reaction of CODH/ACS with excess CO is not over after the first observed single-exponential decay, which is the only change that is kinetically competent for CO oxidation. Since only 0.3 spin of B_{red} per CODH dimer is reduced in the first exponential decay, the remaining absorbance change that occurs over long incubation times results from further reduction of cluster B to form up to 0.6 spin of B_{red} per CODH/ACS dimer. After 15 min the absorbance at 420 nm levels off with a total extinction coefficient change of 8000−10 000 $M^{-1}\ s^{-1}$, or about 60% (9000/14 700) of the total coefficient change from the static measurements. The CODH samples used in stopped-flow kinetics and in the titrations were partially reduced and exhibited 0.25 spin of the EPR signal for B_{red} per CODH dimer.

[5] Another possibility is that C_{ox}, the EPR-silent state of cluster C, binds the second CO molecule. The maximal intensity for C_{red1} is ~0.3−0.4 spin per CODH/ACS dimer, leaving ~60% of the clusters in the C_{ox} state. This proposal would require the inclusion of a second catalytic cycle in parallel with the one shown in Scheme 1 with all redox states being one electron more oxidized. This possibility is unlikely since the EPR and Mössbauer data (Hu *et al.*, 1996) indicate that this proportion (60%) of C_{ox} is catalytically inactive and cannot be reduced to C_{red1} or C_{red2} upon incubation with CO. Furthermore, the C_{ox}/C_{red1} redox potential ($E^{o\prime} = -220$ mV) is outside the range of the redox potentials for CO ($E^{o\prime} = -560$ mV) or ferredoxin ($E^{o\prime} = -440$ mV) reduction. For these reasons, C_{ox} was not included in Scheme 1. When CODH/ACS is fully in the C_{ox} state, ~30−40% of the molecules can enter the catalytic cycle by reduction to the C_{red1} state.

Electron transfer from $C_{red2}-CO$ to cluster B and to X_{ox} is the fourth step in the mechanism in Scheme 1. Although this is treated as a single step, it could be separated into two steps (eqs 9 and 10). Even more steps could be included to

$$[C_{red2}-CO,B_{ox},X_{ox}] \rightleftharpoons [C_{red1}-CO,B_{red},X_{red}] \quad (9)$$

$$[C_{red1}-CO,B_{red},X_{red}] \rightleftharpoons [C_{red2},B_{red},X_{red}] + CO_2 \quad (10)$$

$$[C_{red2}-CO,B_{ox},X_{ox}] \rightleftharpoons [C_{int}-CO,B_{red},X_{ox}] \rightleftharpoons [C_{red1}-CO,B_{red},X_{red}] \quad (11)$$

replace equation 10, with the internal electron transfers occurring in two separate steps (eq 11). Although including these additional intermediate states ($C_{red1}-CO$ and $C_{int}-CO$) in the mechanism may have some heuristic value, these states would need to have very short half-lives since we do not observe the decay of the C_{red2} EPR signal after its initial formation from C_{red1}. Including these steps also does not result in improvements in our kinetic fits and simulations. A simulation (not shown) in which the fourth step was replaced with eqs 9 and 10 and using rate constants of 190 s^{-1} and 450 s^{-1} (value of k_2 at 5 °C), respectively, yielded the same overall rate constant for electron transfer from $C_{red2}-CO$ to B_{ox} and X_{ox} ($k_4 = 130$ s^{-1} at 5 °C) as with the single step 4 shown in Scheme 1. In addition, whether a single step 4 or two steps are included, the intensity of C_{red2} is not predicted to significantly decay and the $C_{red1}-CO$ state should not significantly accumulate.

Implications of the Microscopic Rate Constants. The binding of CO to cluster C_{red1} (expressed as K_{d1}) is remarkably tight and approaches the physiological CO concentration observed in *C. thermoaceticum* cell cultures grown in glucose and CO_2, which is less than 3 μM (Diekert *et al.*, 1984). Under these conditions the accumulating species of CODH/ACS is $[C_{red1},B_{ox},X_{ox}]$. On the other hand, CO binds relatively weakly to cluster C_{red2}, yielding values of K_{d3} that are comparable with the K_m values for CO measured by steady-state kinetics (Table 1). Under k_{cat}/K_{mCO} conditions, the accumulating form of CODH/ACS will thus be C_{red2}. In addition, the rate of conversion of C_{red1} to C_{red2} (k_2) is 10−50-fold faster than k_{cat}, and the values of k_2/K_{d1} are 500−1000-fold higher than k_{cat}/K_{mCO}. These combined observations strongly suggest that the states $[C_{red1},B_{ox},X_{ox}]$ and $[C_{red1}-CO,B_{ox},X_{ox}]$ in Scheme 1 *do not* accumulate during steady-state turnover. Therefore, since the steady-state turnover of CO oxidation follows a ping-pong mechanism, the state $[C_{red2},B_{ox},X_{ox}]$ should be viewed as the "oxidized" form of the enzyme to which CO binds and the state $[C_{red2},B_{red},X_{red}]$ as the two-electron "reduced" form to which CO_2 binds.

To obtain a clearer picture of the distribution of enzyme species during the pre-steady-state and steady-state phases of CO oxidation, preliminary simulations of the steady-state kinetics of CO oxidation with *C. thermoaceticum* FdII as the electron acceptor, using the mechanism in Scheme 1 and the simulated rate constants from Table 1, are shown in Figure 6. During pre-steady state with 1 μM CO, the $[C_{red2},B_{ox},X_{ox}]$ state (labeled F) accumulates to approximately ~90% of the total CODH/ACS concomitant with the decay of $[C_{red1},B_{ox},X_{ox}]$ (labeled E), and then it decreases to 65% of the total enzyme as forms G and H accumulate once steady state is reached (after 500 ms). In contrast, with 970 μM

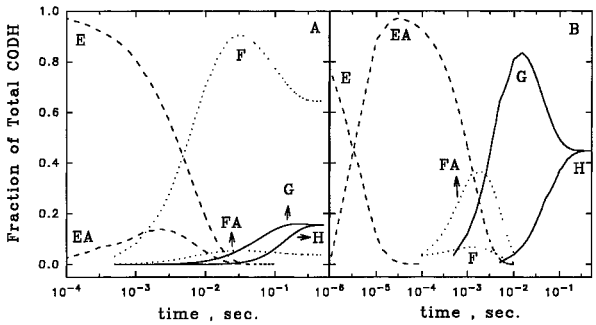

FIGURE 6: Simulation of CODH/ACS intermediates during pre-steady state using the rate constants at 25 °C from Table 1 and the following initial concentrations: 10 nM CODH/ACS dimer, 1.0 μM Fd_{ox}, 0 CO_2, 0 Fd_{red}, and 1.0 μM CO (panel A) or 970 μM CO (panel B). Nomenclature assignments for CODH/ACS intermediates in Scheme 1 are as follows: E, $[C_{red1},B_{ox},X_{ox}]$; EA, $[C_{red1}-CO,B_{ox},X_{ox}]$; F, $[C_{red2},B_{ox},X_{ox}]$; FA, $[C_{red2}-CO,B_{ox},X_{ox}]$; G, $[C_{red2},B_{red},X_{red}]$; H, $[C_{red1},B_{red},X_{red}]$. Values of k_5 and k_6 were assumed to be twice the value of k_{cat} from steady state.

CO (the concentration used in steady-state assay solutions) and 1 μM FdII, the two accumulating states are $[C_{red2},B_{red},X_{red}]$ (labeled G)and $[C_{red1},B_{red},X_{red}]$ (labeled H)—each state is present at 45% during steady state. The states $[C_{red1},B_{ox},X_{ox}]$ and $[C_{red1},B_{ox},X_{ox}]$ (E and EA) deplete completely after 10 ms. Neither of these states accumulates under any set of CO and FdII concentrations. Since the states F and H are at the same redox state, we speculate that H must correspond to $[C_{red1},B_{red},X_{red}]$. This state is formed from $[C_{red2},B_{ox},X_{ox}]$ at a rate much slower than k_3, but it would indeed accumulate if [CODH] ≫ [CO]. The concentration of CODH greatly exceeds that of CO.

Therefore, internal electron transfer from C_{red2} to cluster B and center X compete with the second cycle of CO binding. At high CO concentrations, state F accumulates and two cycles of CO binding and oxidation predominate. However, at low concentrations of CO, internal electron transfer is favored over CO binding, resulting in one cycle of CO oxidation per turnover.

The above conclusions help to rationalize previous inhibition studies of CO oxidation by CODH/ACS. Inhibitors like sodium azide and sodium thiocyanate were shown by EPR (Seravalli *et al.*, 1995) and electron spin echo modulation EPR spectroscopies (Kumar *et al.*, 1995) to bind to cluster C_{red1}. However, they will compete with CO for cluster C_{red2} during CO oxidation. This explains why, when thiocyanate inhibition was studied (Seravalli *et al.*, 1995), the inhibition constant was 36 mM for k_{cat}/K_m^{CO} while its K_d, as monitored by the EPR changes of C_{red1}, was 6 mM. We did not observe any EPR spectroscopic changes on the C_{red2} state of CODH/ACS. Complete inhibition was not possible to achieve at saturating thiocyanate concentrations, since the anionic inhibitors bind to C_{red1} and not to C_{red2}, which would accumulate during steady state.

If all the elementary steps of the mechanism are kinetically competent, all first-order forward rate constants must be higher than the steady-state k_{cat} for the forward direction, and all second-order forward rate constants must be higher than the steady-state k_{cat}/K_m for the forward direction. Accordingly, the forward first-order rate constants shown in Table 2 (k_2 and k_4) are higher than the k_{cat} values (Table 1) at each temperature, and the forward second-order rate constants (k_2/K_{d1} and k_4/K_{d3}) are higher than the $(k_{cat}/K_m)_{CO}$ values. As noted above, k_2/K_{d1} is much higher than both

k_{max}/K_d and $(k_{cat}/K_m)_{CO}$ and are therefore not rate-limiting. However, the k_4/K_{d3} values agree well with k_{max}/K_d for CO (Table 1) and are only 2−4 times higher than $(k_{cat}/K_m)_{CO}$. We conclude that the first reductive half-reaction can be accounted for by the first four steps outlined in Scheme 1, and its rate-limiting step is characterized by k_4/K_d.

For k_{cat}, the rate-limiting step is the two electron transfer steps from CODH/ACS to Fd (k_5 and k_6 in Scheme 1), since k_4 is 5−10-fold higher than k_{cat}. At 25 °C, k_4 (500 s^{-1}) is only 20% rate-determining for k_{cat} (100 s^{-1}), and electron transfer to oxidized FdII is 80% rate-limiting, with a value between 100 and 150 s^{-1}.

Relationship between CODH/ACS Titrations and Pre-Steady-State Kinetics. To explain the titrations of cluster B, we proposed the existence of a fourth redox site in CODH/ACS called S, which is capable of accepting two electrons per center S. On the other hand, the FQ-EPR data suggested involvement of a site called X_{ox}, which is capable of accepting only one electron per center X. Since neither S or X_{ox} exhibits UV−visible absorption changes upon reduction and has a redox potential similar to that of cluster B, it is possible that S is actually a pair of redox sites. In this case, each site is accepting 0.5 equiv of electrons, the product of which would either undergo dimer formation or disproportionation, as shown by eqs 12 and 13. A likely candidate

$$X_{red} + X_{red} \rightleftharpoons S \qquad (12)$$

$$X_{red} + X_{red} \rightleftharpoons X_{ox} + X_{red}^{(2-)} (=S) \qquad (13)$$

for S is a pair of low-potential cysteine residues. According to our simulations, two CO oxidation turnovers are equivalent to 0.6 CO equiv or 1.2 electrons per CODH/ACS dimer, the amount of CO required to titrate cluster B and center S (intersection of the two lines in panel B of Figure 2). The product state of the reductive half-reaction is 0.3 spin of $[C_{red2},B_{red},X_{red}]$ per CODH/ACS dimer. This state could slowly (compared to the rates of pre-steady-state kinetics) undergo internal electron transfer to form 0.3 spin of $[C_{red1},2B_{red},2X_{red}]$ per CODH/ACS dimer (state H in Scheme 1), which, according to eqs 12 and 13, would exhibit no EPR signals from center S but a total of 0.6 spin of B_{red} per CODH/ACS dimer, the maximum titratable amount of cluster B. This explains why, under the equilibrium conditions of the titrations (thermodynamic control), cluster B and center S were reduced before C_{red1} was reduced to C_{red2}, since their redox potentials are higher than the C_{red1}/C_{red2} couple ($E^{o\prime}$ = −520 mV). During pre-steady-state kinetics (kinetic control), C_{red1} will be reduced first to C_{red2} because it is the initial step of CO oxidation. Thus, the first product of the CO titration, and the only product of the dithionite titration is the CODH/ACS state $[0.3C_{red1},0.6B_{red},0.3S_{red}]$. The reduced center S ($S_{red}$) then should accumulate with the same intensity as C_{red1} and C_{red2}. Further experiments are required to identify centers X and S and determine the rate constants for internal electron transfer from cluster C to cluster B in CODH/ACS.

REFERENCES

Anderson, M. E., & Lindahl, P. A. (1994) *Biochemistry 33*, 8702−8711.

Anderson, M. E., & Lindahl, P. A. (1996) *Biochemistry 35*, 8371−8380.

Anderson, M. E, DeRose, V. M., Hoffman, B. M., & Lindahl, P. A. (1993) *J. Am. Chem. Soc. 115*, 12204−12205.

Andreesen, J. R., Schaupp, A., Neurater, C., Brown, A., & Ljundahl, L. G. (1973) *J. Bacteriol. 114*, 743−751.

Barshop, B. A., Wrenn, R. F., & Frieden, C. (1983) *Anal. Biochem. 130*, 134−145.

Bhatnagar, L., Krzycki, J. A., & Zeikus, J. G. (1987) *FEMS Microbiol. Lett. 41*, 337−343.

Bott, M., & Thauer, R. K. (1989) *Z. Naturforsch. 44*, 392−396.

Diekert, G. B., & Thauer, R. K. (1978) *J. Bacteriol. 136*, 597−606.

Diekert, G., Hansch, M., & Conrad, R. (1984) *Arch. Microbiol. 138*, 224−228.

Elliot, J. I., & Brewer, J. M. (1978) *Arch. Biochem. Biophys. 190*, 351−357.

Fan, C., Gorst, C. M., Ragsdale, S. W., & Hoffman, B. M. (1991) *Biochemistry 30*, 431−435.

Fuchs, G. (1986) *FEMS Microbiol. Rev. 39*, 181−213.

Gorst, C. M., & Ragsdale, S. W. (1991) *J. Biol. Chem. 266*, 20687−20693.

Hu, Z. G., Spangler, N. J., Anderson, M. E., Xia, J. Q., Ludden. P. W., Lindahl, P. A., & Münck, E. (1996) *J. Am. Chem. Soc. 118*, 830−845.

Kumar, M., & Ragsdale, S. W. (1992) *J. Am. Chem. Soc. 114*, 8713−8715.

Kumar, M., & Ragsdale, S. W. (1996) *Chem. Rev. 96*, 7, 2515−2539.

Kumar, M., Lu, W.-P., Liu, L., & Ragsdale, S. W. (1993) *J. Am. Chem. Soc. 115*, 11646−11647.

Kumar, M., Lu, W.-P., Smith, A., Ragsdale, S. W., & McCracken, J. (1995) *J. Am. Chem. Soc. 117*, 2939−2940.

Lindahl, P. A., Münck, E., & Ragsdale, S. W. (1990a) *J. Biol. Chem. 265*, 3873−3879.

Lindahl, P. A., Ragsdale, S. W., & Münck, E. (1990b) *J. Biol. Chem. 265*, 3880−3888.

Ljungdahl, L. G. (1986) *Annu. Rev. Microbiol. 40*, 415−450.

Lu, W.-P., & Ragsdale, S. W. (1991) *J. Biol. Chem. 266*, 3554−3564.

Menon, S., & Ragsdale, S. W. (1996) *Biochemistry 35*, 12119−12125.

Qiu, D., Kumar, M., Ragsdale, S. W., & Spiro, T. G. (1994) *Science 264*, 817−819.

Qiu, D., Kumar, M., Ragsdale, S. W., & Spiro, T. G. (1995) *J. Am. Chem. Soc. 117*, 2653−2654.

Qiu, D., Kumar, M., Ragsdale, S. W., & Spiro, T. G. (1996) *J. Am. Chem. Soc. 118*, 10429−10435.

Ragsdale, S. W. (1991) *CRC Crit. Rev. Biochem. Mol. Biol. 26*, 261−300.

Ragsdale, S. W., Ljungdahl, L. G., & DerVartanian, D. V. (1982) *Biochem. Biophys. Res. Commun. 108*, 658−663.

Ragsdale, S. W., Clark, J. E., Ljungdahl, L. G., Lundie, L. L., & Drake, H. L. (1983) *J. Biol. Chem. 258*, 2364−2369.

Ragsdale, S. W., Wood, H. G., & Antholine,W. E. (1985) *Proc. Natl. Acad. Sci. U.S.A. 82*, 6811−6814.

Santiago, B., & Meyer, O. (1996) *FEMS Microbiol. Lett. 142*, 309−310.

Seravalli, J., Kumar, M., Lu, W.-P., & Ragsdale, S. W. (1995) *Biochemistry 34*, 7879−7888.

Shin, W., & Lindahl, P. A. (1992) *Biochemistry 31*, 12970−12875.

Shin, W., Stafford, P. R., & Lindahl, P. A. (1992) *Biochemistry 31*, 6003−6011.

Thauer, R. K., Fuchs, G., Käufer, B., & Schnitker, U. (1974) *Eur. J. Biochem. 45*, 343−349.

Valentine, J. S. (1994) in *Bioinorganic Chemistry* (Bertini, I., *et al.*, Eds.) Chapter 5, pp 276−283, University Science Books, Mill Valley, CA.

Xia, J., Dong, J., Wang, S., Scott, R. A., & Lindahl, P. A. (1995) *J. Am. Chem. Soc. 117*, 7065−7070.

Xia, J. Q., Sinclair, J. F., Baldwin, T. O., & Lindahl, P. A. (1996) *Biochemistry 35*, 1965−1971.

Zimmerle, C. T., & Frieden, C. (1989) *Biochem. J. 258*, 381−387.

BI970590M